Quantum Spin Fluctuations and Hydrogen Bond Network in the Antiferromagnetic Natural Mineral Henmilite – Supplemental Material –

Hajime Yamamoto,[1] Terutoshi Sakakura,[1] Harald O. Jeschke,[2] Noriyuki Kabeya,[3] Kanata Hayashi,[4] Yuya Ishikawa,[4] Yutaka Fujii,[4] Akira Ochiai,[3] Shunji Kishimoto,[5] Hajime Sagayama,[5] Kei Shigematsu,[6] Masaki Azuma,[6] Yukio Noda,[1] and Hiroyuki Kimura[1]

[1]*Institute of Multidisciplinary Research for Advanced Materials, Tohoku University, Katahira 2-1-1, Aoba, Sendai 980-8577 Japan*
[2]*Research Institute for Interdisciplinary Science, Okayama University, Okayama 700-8530, Japan*
[3]*Department of Physics, Tohoku University, Aoba 6-3, Aoba, Sendai 980-8577, Japan*
[4]*Research Center for Development of Far-Infrared Region, University of Fukui, Bunkyo 3-9-1, Fukui 910-8507, Japan*
[5]*Photon Factory and Condensed Matter Research Center, Institute of Materials Structure Science, High Energy Accelerator Research Organization, Oho 1-1, Tsukuba 305-0801, Japan*
[6]*Laboratory for Materials and Structures, Tokyo Institute of Technology Nagatsuta 4259, Midori, Yokohama 226-8503, Japan, Kanagawa Institute of Industrial Science and Technology (KISTEC), Ebina 243-0435, Japan*

(Dated: September 3, 2021)

I. CRYSTAL STRUCTURE REFINEMENT

Details of the SXRD data collection and crystal structure information for henmilite. To determine the crystal structure of henmilite, a four-circle diffractometer at BL-14A, Photon Factory, was used to collect data for refining the lattice and structural parameters. The refined parameters are summarized in TABLE S1 and the Crystallographic Information File (CIF). Each O-H bond and O-O bond lengths are summarized in TABLE S2. The bond lengths were analyzed using the VESTA software.

Phase purity of the henmilite samples. To confirm the phase purity of henmilite samples, synchrotron X-ray powder diffraction was performed at BL-8B, Photon Factory (FIG. S1). The atomic position parameters are fixed from the

TABLE S1. Lattice parameters and details of the SXRD data collection of henmilite.

Crystal data	
Space group	$P\bar{1}$
a (Å)	11.538(2)
b (Å)	7.989(3)
c (Å)	5.6504(12)
α (°)	109.68(2)
β (°)	91.516(17)
γ (°)	83.710(19)
V (Å^3)	487.4(2)
Z	2
Crystal radius (μm)	70
$r_{\rm calc}$ (g cm^{-3})	2.5171
wavelength (Å)	0.68431(2)
μ (mm^{-1})	3.009
Data collection and Refinement	
$2\theta_{\rm max}$ (°)	131.4
unique data	9059
Data with $I_o > 3s(I_o)$	8215
Variables	192
R	0.0176
wR	0.0422
S	1.68

TABLE S2. Determined O-H bond and O-O bond lengths.

Atom No.	O-H bond (Å)	O-O bond (Å)
O1-H1···O7	0.764(9)	2.9079(6)
O2-H2···O1	0.782(10)	3.0577(6)
O3-H3···O1	0.818(13)	3.2853(7)
O4-H4···O2	0.809(13)	3.3131(6)
O5-H5···O2	0.775(11)	2.8418(6)
O6-H6···O1	0.733(11)	2.7844(5)
O7-H7···O8	0.765(10)	2.7977(6)
O8-H8···O2	0.718(10)	3.0130(6)
O9-H9···O12	0.798(13)	2.7884(6)
O10-H10···O11	0.791(13)	2.7809(6)
O11-H11···O6	0.703(14)	2.8433(5)
O12-H12···O5	0.696(14)	2.8371(5)

single crystal data. Some henmilite crystals were crushed into the powder. No impurity phase was observed in the henmilite samples.

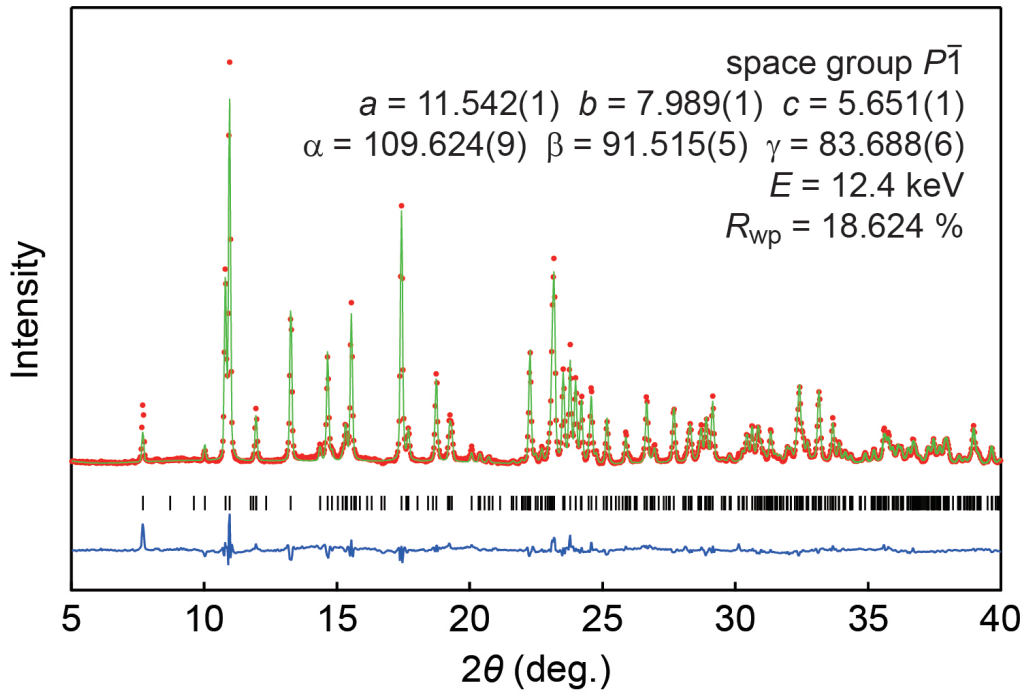

FIG. S1. Synchrotron X-ray powder diffraction pattern and result of Rietveld analysis of the henmilite sample.

II. MAGNETIC MEASUREMENTS

FIG. S2 shows the magnetic field dependence of magnetization at 2 and 4 K. A slight inflection point associated with a short-range ordering was observed around 3 T, while the nonlinearity vanishes completely at 4 K.

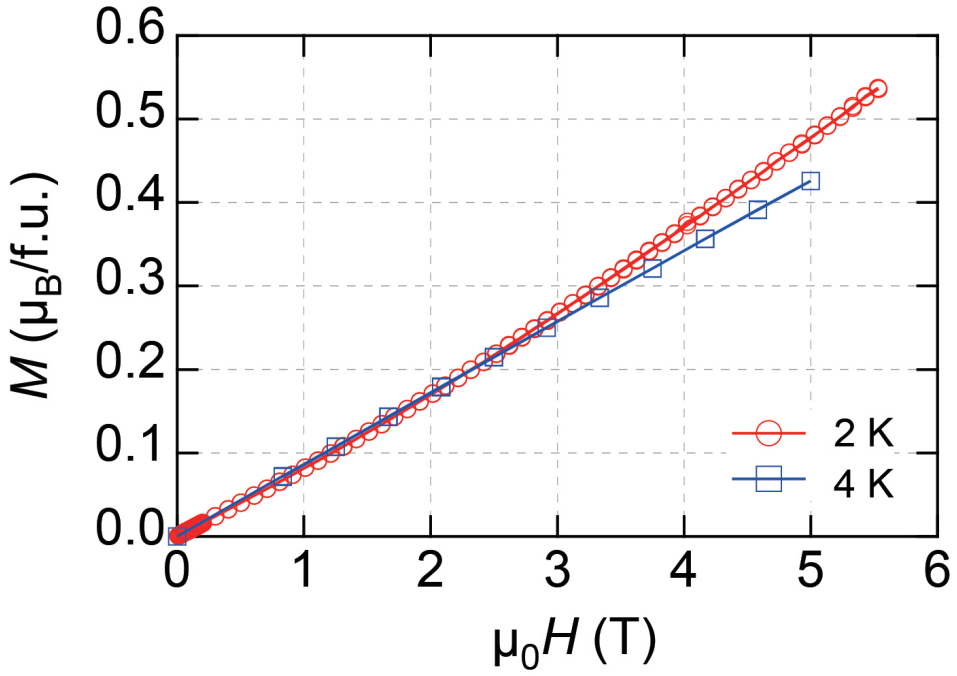

FIG. S2. Magnetic field dependence of magnetization at 2 and 4K.

III. HEAT CAPACITY MEASUREMENTS

The nuclear contribution to the specific heat is estimated by the equation $C = B\,T^{-2}$, where C is the heat capacity, B is a coefficient, and T is the temperature. The subtraction process at 0 T is shown in Fig. S3.

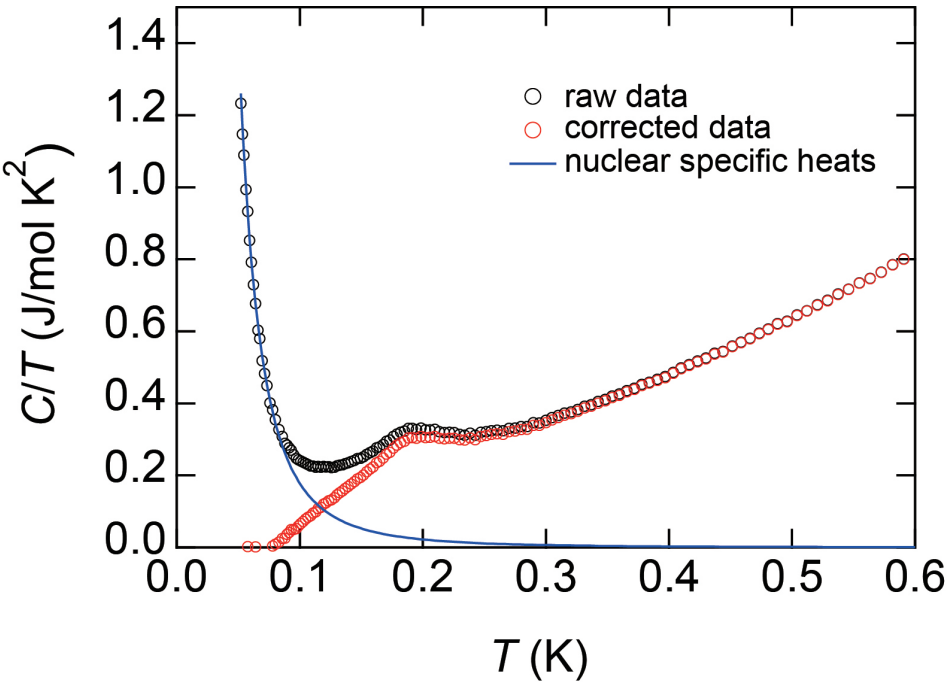

FIG. S3. Subtraction procedure of the nuclear contribution to the specific heat.

IV. ADDITIONAL DENSITY FUNCTIONAL THEORY RESULTS

In Table S3, we provide all Heisenberg Hamiltonian parameters obtained by the energy mapping method. The line given in bold face is obtained by interpolation and matches the experimental Curie-Weiss temperature.

TABLE S3. Exchange couplings of $Ca_2Cu(OH)_4[B(OH)_4]_2$, calculated within GGA+U and $2 \times 2 \times 2$ k points ($U = 7\,\text{eV}$ and $U = 8\,\text{eV}$ with $4 \times 4 \times 4$ k points). The experimental value $T_{\text{CW}} = -3.0$ K of the Curie Weiss temperature is matched by the line in bold face. Statistical errors are indicated. Exchange couplings are identified by Cu-Cu distances given in the last row.

U (eV)	J_1 (K)	J_2 (K)	J_3 (K)	J_4 (K)	J_6 (K)	J_8 (K)	J_9 (K)	T_{CW} (K)
6	4.97(1)	4.55(3)	1.02(2)	0.19(3)	-0.01(2)	0.30(2)	0.28(2)	-4.07
6.5	4.51(1)	4.21(1)	0.97(1)	0.17(1)	-0.01(1)	0.27(1)	0.26(1)	-3.72
7	4.11(1)	3.90(1)	0.94(1)	0.16(1)	-0.01(1)	0.24(1)	0.23(1)	-3.42
7.5	3.75(1)	3.61(1)	0.91(1)	0.15(1)	0.00(1)	0.22(1)	0.20(1)	-3.14
7.747	**3.59(1)**	**3.48(1)**	**0.89(1)**	**0.14(1)**	**0.00(1)**	**0.20(1)**	**0.19(1)**	**-3.0**
8	3.43(1)	3.35(1)	0.87(1)	0.14(1)	0.00(1)	0.19(1)	0.18(1)	-2.90
8.5	3.15(1)	3.10(1)	0.85(1)	0.14(1)	0.00(1)	0.17(1)	0.16(1)	-2.68
d_{Cu-Cu} (Å)	5.6504	5.73196	5.80678	7.89737	8.03803	8.16588	8.19733	